Fractionation of REE, U, and Th in natural ore-forming hydrothermal systems: Thermodynamic modeling

A. Migdisov[1*], X. Guo[2], H. Nisbet[1], H. Xu[1], and A.E. Williams-Jones[3]

1. Earth and Environmental Sciences Division, Los Alamos National Laboratory, P.O. Box 1663, M.S. J535, Los Alamos, NM 87545, USA

2. Department of Chemistry and Alexandra Navrotsky Institute for Experimental Thermodynamics, Washington State University, Pullman, WA 99164

3. Department of Earth and Planetary Sciences, McGill University, 3450 University Street, Montreal, Canada, H3A 0E8

---

*artas@lanl.gov

Abstract:

This contribution presents a thermodynamic model revealing the mechanisms responsible for separation of Heavy and Light Rare Earth (HREE and LREE) phosphates in natural hydrothermal systems at temperatures of 250-350 °C. Our calculations were performed for an
5   isothermal column of rock containing 0.5 wt% of apatite (Ca phosphate), which served as an immobilizing agent for REE dissolved in the solution. REE were transported by 10 wt% NaCl acidic solution. The model accounted for formation of REE phosphate solid solutions through a regular mixing model. It demonstrates that hydrothermal flushing can efficiently separate REE forming xenotime (HREE phosphate solid solutions) at the beginning of the column, and re-
10 transportation of monazite (LREE rich) to the end of the column. This separation is primarily due to the fact that at elevated temperatures stability LREE chloride complexes is significantly higher than that for HREE. The model also evaluates behavior of U and Th, which accompany REE in vast majority of natural locations. It was found that U strongly fractionates to xenotime, whereas Th fractionates to monazite. This phenomenon can be explained by the differences in crystal-
15 chemical characteristics between monazite and xenotime, and the mobility of Th in aqueous solutions at elevated temperatures.

1. Introduction

Development of new technologies, particularly those designed to address environmental concerns, and those that are essential for renewable energy applications (such as wind turbines, solar panels, electric cars, and advanced batteries), has called for a great demand in Rare Earth Elements (REE) materials. The global production of REE, however, is largely restricted to a single country (China), and thus supplies of these elements are vulnerable to political and/or economic decisions that are beyond the control of global markets. As these elements are critical for the future economy, there has been considerable pressure to find new sources [1]. In the US alone, the annual REE consumption currently approaches 20,000 metric tons [2], and meeting such a scale of demand most likely requires sustainable domestic mining, which, in turn, suggests that either new natural sources of REE (new ore deposits) have to be found, or new technologies must be developed for more efficient extraction of these elements from existing sources. These goals (at least with regards to finding new sources) cannot be achieved without quantitative understanding of chemical mechanisms responsible for transport, fractionation, and concentration of REE in natural processes leading to the formation of natural REE deposits.

It is now almost universally agreed that hydrothermal fluids commonly mobilize the REE and concentrate to economic levels. Thus, besides the need for basic REE science, understanding the behavior of REE in hot aqueous solutions circulating in Earth's crust is required for developing tools to discover new economic REE supplies. Recently, we have summarized thermodynamic data currently available on the behavior of REE in hydrothermal systems and proposed a set of models, evaluating the main controls of the formation of monazites and xenotimes (REE-phosphates, one of the main ore minerals supplying REE to industry) from natural solutions [3]. These models suggest the mobilization of REE in natural hydrothermal systems occurs primarily in acidic (pH<3) solutions rich in chloride- and sulfate, and depleted in fluoride- and phosphate, carrying REE in concentrations of up to several hundred ppm [4]. REE deposition is related to the encounter of these solutions with rocks containing apatite (Ca-phosphate). These models additionally investigated, to the first approximation, the conditions at which these processes can lead to the separation of Medium and Heavy REE (M/HREE) which are highly sought out in industry, from the less economically attractive Light REE (LREE).

It should be noted, however, that the models proposed in Migdisov et al. [3] are highly approximate. Mainly, the calculations reported did not account for the ability of REE phosphates to form multi-component solid solutions, where deposition and fractionation of the REE was modelled through corresponding pure end-member REE phosphates. This is a significant deficiency in the model: natural monazites and xenotimes always form solid solutions, which are more complex than end members [5]. Monazite solid solutions, which adopt a monoclinic structure (space group $P2_1/n$, Figure 1-left), are predominated [6] by Ce, La, or Nd phosphates (Ce-, La-, and Nd-monazites, respectively) and can effectively incorporate all L/MREE (down to Gd) together with U and Th [7]. Xenotime solid solutions that possess a tetragonal structure (space group $I4_1/amd$, Figure 1-right), are typically predominated by Y phosphates and contain mostly HREE together with U and Th [8]. The monazite structure is comprised of chains of alternating [PO_4] tetrahedra, and nine-fold coordinated REE and substituted U/Th (Fig. 1-left). The xenotime structure is of zircon ($ZrSiO_4$) type, consisting of eight-coordinated REE/U/Th site and [PO_4] (Fig. 1-right). The differences between the two structures result in their different preferences for REE/U/Th: monazite favors L/MREE and Th, while xenotime favors HREE and U. This behavior can simply be interpreted by the size effect of substituting ions, i.e., the larger
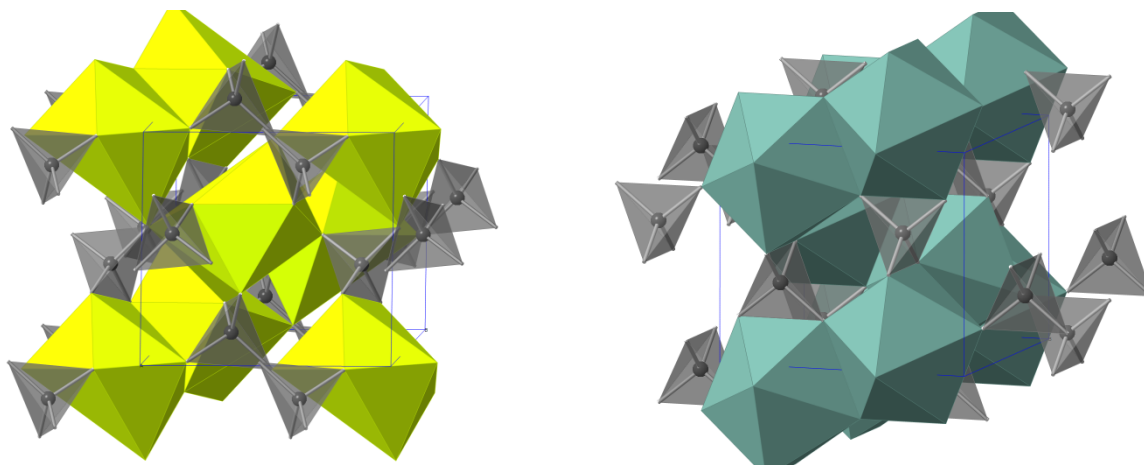
3

Figure 1. Crystal structures of monazite (left) and xenotime (right). The figures are drawn based on the structure data of CePO$_4$ (left) and YPO$_4$ (right) [6]. Grey tetrahedron represents [PO$_4$], yellow polyhedron represents [CeO$_9$] and blue polyhedron represents [YO$_8$]. Blue lines denote the unit cell.

L/MREE and Th prefer the larger nine-fold coordinated site in monazite and the smaller HREE and U prefer the smaller eight-fold coordinated site in xenotime [9]. However, due to the varying sizes among L/MREE/Th or HREE/U, their monazite or xenotime solid solutions expectedly exhibit non-ideal mixing behavior. As a result, reactivity of solid solution components can be significantly different from that of individual end-members, and can therefore modify or shift the main trends observed in end-member phases [3]. In addition, these models do not account for the occurrence of U and Th, whose presence (up to 20 wt %) in monazite and xenotime poses significant problems for the REE mining industry as radioactive elements require special measures to be taken for their treatment and disposal, significantly increasing the REE recovery costs [10–12]. On the other hand, being the primary REE-bearing ore mineral, monazite with an elevated content of Th, is also the main Th ore mineral, and with respect to the Th mining industry, the role of Th in monazite shifts from a highly unwelcome contaminant to a main mining commodity. Hence, development of thermodynamic models that predict the formation of both U/Th-enriched and U/Th-depleted monazite/xenotime is crucial for the discovery of new, economically feasible, resources of REE while fulfilling the needs of Th-mining industry.

In this contribution, we attempt to expand the calculations reported in Migdisov et al. [3] by incorporating solid solution models for monazites/xenotimes and by accounting for the mobility of U and Th in aqueous solutions. We propose a first, though approximate, evaluation of the mechanisms that potentially can be responsible for natural separation of REE and actinides.

2. Description of the model

The model presented here simulates progressive hydrothermal alteration and re-distribution of REE, U, and Th by acidic solutions in a one-dimensional column of a rock containing 0.5 wt% apatite, which was evaluated using the step-flow reactor approach ("box-model"). The scenario evaluated in our model is illustrated in Figure 2. The initial event ("step 1") involved interaction and equilibration of a 1 kg aliquot of the solution carrying REE, U, and Th with 1 kg of rock,
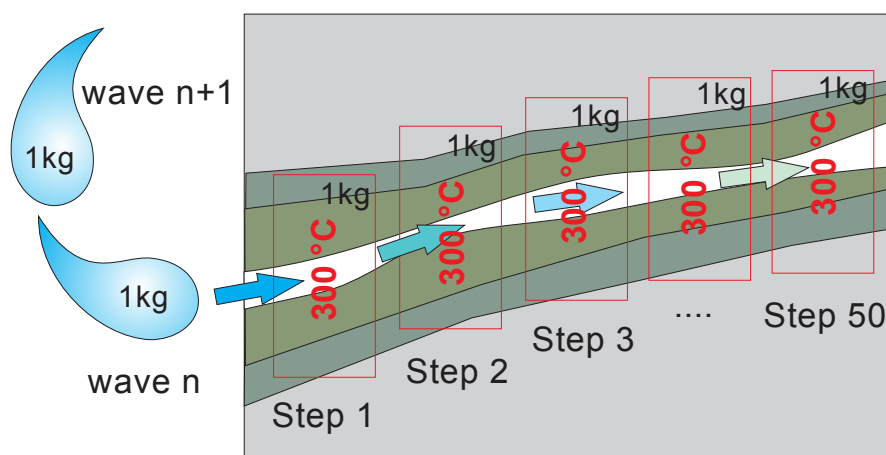
4

Figure 2. A sketch of the model calculated to evaluate fractionation of REE, U, and Th after interaction of a 10 wt.% NaCl solution carrying these elements with a rock containing 0.5 wt% apatite

resulting in the deposition of monazite/xenotime minerals. This equilibrated fluid was moved to the second reactor where it was equilibrated with 1 kg of fresh, unaltered rock; the resulting fluid was subsequently moved to the next reactor once again containing 1 kg of fresh, unaltered rock. This operation procedure was repeated 50 times, creating a column of rock altered by the first passage of the fluid aliquot ("wave 1"). After completion of the first "wave", a new portion of fluid (1 kg) of the same composition, was flushed through the already altered column in an identical manner ("wave 2"), as described above. The number of "waves" evaluated in the model ranged from 5 to 50; this computational technique is one of the simplest approaches to evaluate the possibility for separation of REE, U, and Th in systems continuously flushed by hydrothermal solutions, allowing for an investigation on the behavior of REE, U, and Th at changing fluid/solid ratios. The models were formulated using the HCh/Unitherm code [13].

Calculations were performed at isothermal conditions of 250, 300, and 350 °C. Temperature selection was based on fluid inclusion homogenization temperatures reported for known REE deposits [4,14–16]. These studies suggest the temperature range of 250–500 °C, which broadly corresponds to the temperature interval of primary relevance for the hydrothermal transport and deposition of REE. However, we have restricted the model to 350 °C to avoid uncertainties associated with long-range temperature extrapolation of thermodynamic properties of aqueous species (see below). In order to avoid alteration of the observed trends by pH, redox, and other buffering parameters of the rock, the latter was assumed to be chemically inert and the only chemically active component of it was apatite. The composition of the solution was set based on compositions documented for solutions associated with natural REE ore forming systems. Fluid inclusion studies indicate that the Bayan Obo deposit in China was formed from brines containing 7 to 10 wt.% NaCl equivalent [14]. The fluids responsible for ore deposition at Gallinas Mountains contained 12 to 18 wt.% NaCl equivalent [15], and the Karonge deposits formed from a brine containing 25 wt.% NaCl equivalent [16]. To avoid uncertainties associated

5

with poorly defined activity models for highly saline brines at elevated temperatures, the solution selected for calculations contained only 10 wt.% NaCl (1.72 mol/kg) and simulated the scenario of re-distribution of REE, U, and Th by fluid containing 10 wt.% NaCl. Concentrations of REE in the solution associated with the initial depositional event ("step 1") were closely approximated to the composition of fluid inclusions from the Capitan Pluton REE mineralization (Table 1), documented by Banks et al. [4].These authors, however, did not report the concentrations of Y, the main component of xenotime solid solutions. Natural occurrence of Y varies significantly; in our calculations, the concentrations of this element were set to be one third of the concentrations of La and Ce. Concentrations of U and Th in these solutions were fixed by their saturation with respect to uraninite (UO_2) and thorianite (ThO_2), respectively, at the temperature of calculations. The value of pH^T of the initial solution was set at ~2 [17] by adding appropriate amounts of HCl. Considering that U is a highly redox sensitive element, the scenario discussed above was modelled at various redox conditions. The most reducing conditions considered in our model corresponded to the Ni/NiO redox buffer: a typical redox condition encountered in reducing natural systems (log fO_2 = -38.06, -33.90, and -30.46, at 250, 300, and 350 °C, respectively). The oxidizing scenario incorporated redox conditions corresponding to the hematite/magnetite (Fe_2O_3/Fe_3O_4) equilibrium (log fO_2 = -35.22, -30.9, and -27.0, at 250, 300, and 350 °C, respectively) or higher (e.g., HM+2: log fO_2 = log fO_2^{HM}+2) – another redox state typical of natural hydrothermal systems. However, Ni and Fe were not included in the chemical description of our system: redox conditions were set directly through the corresponding fugacity of O_2^{gas}; in these calculations, oxygen did not obey the mass balance law and its behavior and content in the system were controlled by the chemical potential of O_2^{gas}. Thus, for each temperature discussed above, calculations were performed for at least two scenarios: 1) starting solution of 10 wt.% NaCl, reducing conditions (Ni/NiO), and 2) starting solution of 10 wt.% NaCl, oxidizing conditions (HM+).

3. Thermodynamic description of the system
3.1. Aqueous speciation

A full list of aqueous species employed in the calculations, together with the parameters of equations of state used to extrapolate their properties to elevated temperature, as well as the data sources, is provided in the Electronic supplement to this paper. All calculations of equilibrium compositions conducted in this study employed Haar-Gallaher-Kell [18] and Marshall and Franck [19] models for calculation of the thermodynamic properties and dissociation constant of H_2O, respectively. The activities of the individual ions were calculated using the extended Debye-Hückel model modified by Oelkers et al. [20] and Oelkers and Helgeson [21] for NaCl-dominated solutions (recommended for up to I = 6 and T up to 600 °C):

$$\log \gamma_i = \frac{A \cdot [Z_i]^2 \cdot \sqrt{I}}{1 + B \cdot \dot{a} \cdot \sqrt{I}} + \Gamma + b_\gamma \cdot I \qquad (1)$$

where A and B are the Debye–Hückel solvent parameters, γ_i, Z_i and $\dot{a}_i$ are the individual molal activity coefficient, the charge, and the distance of closest approach of an ion i, respectively. The effective ionic strength calculated using the molal scale is I, Γ is a molarity to molality conversion factor, and b_γ is the extended-term parameter for NaCl from Oelkers et al. [20] and Oelkers and Helgeson [21].

Thermodynamic properties of basic aqueous species $O_2^o{}_{aq}$, $H_2^o{}_{aq}$, Na^+, $NaOH^o{}_{aq}$, $NaHS^o{}_{aq}$, $NaSO_4^-$, $NaCl^o{}_{aq}$, and Cl^- were taken from Johnson et al. [22], Shock et al. [23], and Sverjensky et al. [24]. The stability of $HCl^o{}_{aq}$ ion pair was evaluated using the combined data from Tagirov et al. [25] and Ho et al. [26]. Thermodynamic properties of O_2^{gas}, which was used to control redox conditions in aqueous solutions, were taken from Holland and Powell [27]. The properties of simple hydrated ions REE^{3+}, Th^{4+}, U^{4+}, and UO_2^{2+} were taken from Shock et al. [23] and [28].

Aqueous complexes of REE: High temperature stability of aqueous REE complexes has been discussed in detail in Migdisov et al. [3]; thus for topics not covered in the following review the readers may refer to this publication.

The stability of *hydroxyl complexes* of REE were modeled using the data reported by Haas et al. [29]. It should be noted that at the acidic pH modelled in our calculations, these species do not contribute significantly to the mass balance of dissolved REE. Moreover, as shown by Wood et al. [30], the data reported in Haas et al. [29] likely overestimates the stability of hydroxyl complexes of REE at elevated temperatures, and therefore its actual contribution could be even lower. The data on the stability of *chloride complexes* of REE at elevated temperatures has been summarized in Migdisov et al. [3]. The available experimental studies have demonstrated that in solutions containing up to 5 M NaCl at temperatures up to 300 °C, the dominant REE chloride complexes are the mono- and dichloride species, $REECl^{2+}$ and $REECl_2^+$. Figure 3 illustrates the inter-element dependencies of thermodynamic stability constants (β^{Cl}_n) for both of these complexes obtained experimentally at different temperatures. It can be seen from this figure that the stability of REE chloride species increases with increasing temperature. For example, the stability of the LREE rises ~2 orders of magnitude for a temperature increase from 150 to 250 °C. The data also shows that the LREE are more stable, and, thus, more mobile than the HREE in chloride-bearing aqueous solutions, and this difference in stability increases with increasing temperature. Given that, in acidic solutions containing 10 wt.% (and higher) NaCl, chloride complexes play a significant role in the mass balance of dissolved REE [3], the higher stability of LREE complexes over HREE complexes is one of the main vehicles for separating LREE from HREE in hydrothermal processes. The stability of Y chloride complexes at hydrothermal temperatures has not yet been determined experimentally nor evaluated theoretically. At ambient conditions, however, the stability of these species was found to be effectively indistinguishable from those
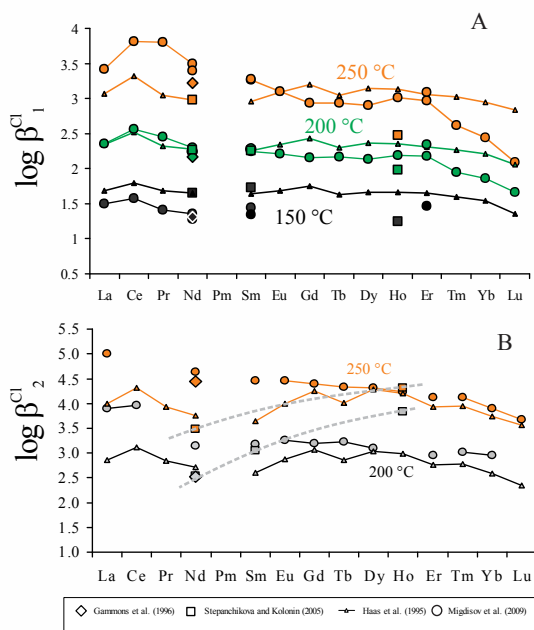

Figure 3. Comparison of the values of the first formation constants (A) and the second formation constants (B) of REE chloride complexes obtained experimentally [91–96] and predicted theoretically (triangles)[29].

determined for chloride complexes of Ho and Dy [31] (which is consistent with the similar ionic radii of these metals: 0.900, 0.901, and 0.912 Å for Y, Ho, and Dy, respectively). Considering the latter, we modelled the behavior of Y chloride complexes assuming them to be identical to Ho chloride complexes. It should be pointed out, however, that this assumption is a very rough first approximation, and that accurate modeling of the behavior of Y in Cl-bearing solutions requires the accumulation of an additional experimental dataset. The data reported in Migdisov et al. [3] is recommended for calculations up to 350 °C; thus, the upper temperature range considered in our calculations was limited to this temperature.

Aqueous complexes of U: During the past several years, a number of studies evaluating the thermodynamics of U aqueous species have been published. Of these studies, a few have theoretically or experimentally derived high temperature stability constants of U species [32–34]. The most recent summary of high temperature stability of U species was reported in [34], from which the majority of the data used in our calculations on the stability of U species were taken; for detailed information, the readers are referred to [34].

The stability of *hydroxyl complexes of U(IV)* was calculated based on the data reported in Shock et al. [28] and summarized in Wang et al. [33]. It should be noted that the derivation of these properties in Shock et al. [28] are primarily based on the experimental study of Parks and Pohl [35]. This study, however, only experimentally determined the stability of UOH^{3+} and $U(OH)_4°$. Stability constants for other hydroxyl species of U(IV) were theoretically extrapolated by Shock et al. [28]. Notably, the values recommended by Parks and Pohl [35] were derived based on the solubility of UO_2 determined in Cl-bearing solutions at temperatures up to 300 °C and strictly reduced conditions. Following the features observed at 25 °C, derivations of the properties of UOH^{3+} and $U(OH)_4°$ were performed by the authors assuming ignorable complexation of U(IV) with chloride. However, the latter assumption is likely erroneous. As it was shown experimentally in Timofeev et al. [36], at T≥250 °C affinity of U(IV) to chloride increases drastically, and in acidic (pH^T = 1.6-2.1) solutions having concentration of NaCl of 0.5-1.5 mol/kg the complex $UCl_4°$ became the predominant species of U(IV) in aqueous solution. The study of Parks and Pohl [35] was performed at low concentrations of chloride and involved pH^T, at which contribution of $UCl_4°$ was significantly lower than that observed in the experiments of Timofeev et al. [36]. Nevertheless, there is still possibility that the data derived for UOH^{3+} (whose stability was derived based on the measurements at low pHT, where chloride complexation might have effect) may overestimate the stability of this species at elevated temperatures.
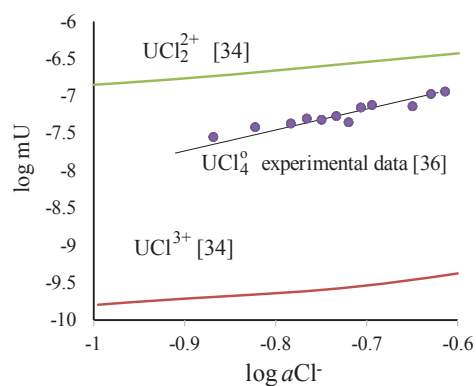

Figure 4. Comparison of predictions made based on the extrapolations reported in Xing et al. [34] with experimental data reported in Timofeev et al. [36]

The stability of *chloride complexes of U(IV)* has been discussed in detail in Xing et al. [34]. The authors used an iso-coulombic extrapolation technique, where, based on the data available for UF^{3+} and UF_2^{2+} [37,38] and low-T data for chloride species of U(IV)

[37,38], they derived temperature dependence of the formation constants for UCl^{3+} and UCl_2^{2+}. In addition, experiments involving the determination of the solubility of U oxides in acidic NaCl solutions at controlled redox conditions [36] have recently revealed that the predominant chloride complex of U(IV) at 250-350 °C is $UCl_4°$; a complex that has not been detected at ambient conditions. To account for this species in our calculations, the formation constants reported in Timofeev et al. [36] for 250, 300, and 350 °C were fitted to the modified Ryzhenko-Bryzgalin model [39] (MRB); the parameters of this equation of state are listed in the summarizing Table available in the Electronic Supplement. In order to test the obtained dataset for U(IV)-chloride complexes, we have modeled species distribution in the system experimentally investigated in Timofeev et al. [36] (up to 1.5 mol/kg NaCl, 300 °C, saturation with respect to solid UO_2, Ni/NiO solid state redox buffer). Extrapolations of Xing et al. [34] suggest an predominance of UCl_2^{2+} under the conditions of the experiments reported by Timofeev et al. [36], whereas the latter suggests the predominance of $UCl_4°$ () and concentrations of dissolved U lower than that predicted by extrapolations. Therefore, we conclude that the extrapolations of Xing et al. [34] overestimate the stability of UCl_2^{2+} and thus we did not account for this species in our calculations.

Experimental studies have identified a large variety of *uranyl-hydroxide complexes* at ambient conditions [32,33]. These include a range of mono-nuclear species varying from UO_2OH^+ to $UO_2(OH)_4^{2-}$, and a range of poly-nuclear species varying from $(UO_2)_2(OH)_2^{2+}$ to $(UO_2)_4(OH)_7^+$. The properties of these complexes were reviewed and extrapolated to elevated temperatures in [34]. The authors [34] noted that their extrapolations suggest the stability of poly-nuclear complexes decrease with increasing temperature. The latter conclusion is in qualitative agreement with our recent experimental findings for the behavior of Th hydroxyl complexes [40]. The stability of *uranyl-chloride complexes* was modeled based on the formation constants obtained experimentally using in situ high-T UV-Vis spectroscopy [41] and solubility techniques [36] at temperatures up to 350 °C. These data indicate that at the conditions of our calculations, chloride speciation of uranyl is controlled by the complexes UO_2Cl^+ and $UO_2Cl_2°$; the latter becoming predominant at T>150-200 °C. In spite of using significantly different experimental techniques in Migdisov et al. and Timofeev et al. [36,41], the data collected are in perfect agreement (). This agreement permits us to assume reasonably good accuracy of the recommended values of formation constants. That said, it should be noted that this dataset is in significant disagreement with a study performed using the Raman spectroscopic technique [42], suggesting much higher affinity of uranyl to chloride and the development of high level chloride species, such as $UO_2Cl_3^-$, $UO_2Cl_4^{2-}$, and $UO_2Cl_5^{3-}$. Nevertheless, taking into account that the speciation model proposed by Dargent et al. [42] has not been confirmed by the study conducted using UV–visible spectroscopy [41], nor the solubility study using the autoclave technique [36], we conclude that the stability constants reported in Dargent et al. [42] are likely overestimated and thus we do not consider them here (for a more detailed discussion on this subject, readers are
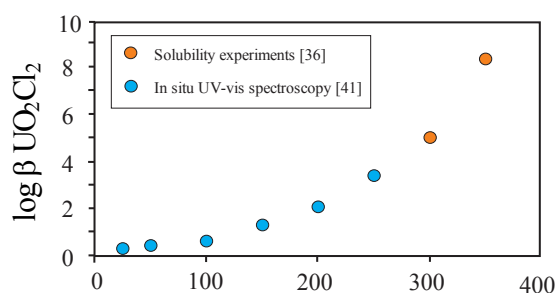

Figure 5. Comparison of the values of formation constants for UO_2Cl_2 complex obtained using in situ UV-vis spectroscopy [41] and autoclave solubility technique [36]

9

referred to Migdisov et al. [43]). Although we do not exclude the possibility that these species may contribute to the mass balance of dissolved U at higher concentrations of NaCl, at the conditions considered in our calculations, their occurrence at significant levels is unlikely.

Aqueous complexes of Th: Information on the stability of aqueous species of Th is much sparser than that available for U. The main source of data currently available is [44]. This compilation however reports stability constants derived only for temperatures below 100 °C: to the best of our knowledge, the only paper to report the formation constants for aqueous complexes of Th at hydrothermal conditions is our recent experimental study [40] on the solubility of ThO_2 in solutions of variable pH ($pH^T = 1.5 - 3.5$) and NaCl concentrations (0-2.5 mol/kg) at temperatures up to 250 °C. Thus, the calculations reported in this contribution are based on high-T extrapolations from the data reported in [44] and the stability constants derived in [40].

At ambient conditions, a number of *Th-hydroxyl complexes* ($Th_x(OH)_y^{4x-y}$), including monomeric (1,1), (2,1), (3,1) and (4,1) species; dimeric (1,2), (2,2), (3,2), (4,2) and (7,2) species; trimeric (3,3), (5,3) and (6,3) species; tetrameric (8,4) and (12,4) species; and hexameric (14,6) and (15,6) species, have been reported in [45]. The degree of contribution of poly-nuclear species to the mass balance of dissolved Th is, however, still under debate: differences in experimental methods, the range of Th concentrations and the ionic media used have made it difficult, if not impossible, to select and interpret the data needed to produce the "best" chemical model[45–48]. Our high temperature study [40], however, suggests that the contribution of poly-nuclear complexes decreases drastically with temperature, and that at T>150 °C, the predominant hydroxyl complexes of Th are mono-nuclear $Th(OH)_2^{2+}$ and $Th(OH)_4°$. In our calculations, complexation of Th with hydroxyl was thus modeled with these species using the recommended formation constants fitted to the MRB model. This study [40] has also demonstrated that the contribution of *Th chloride complexes* to the mass balance of dissolved Th is undetectable at NaCl concentrations of up to 2.5 mol/kg and temperatures up to 250 °C ().
Considering the latter and complete absence of any information on the stability of these complexes at elevated temperatures, chloride complexes of Th were not considered in our calculations.

Figure 6. Solubility of ThO_2 determined as a function of increasing NaCl content [40] at (a) 175, (b) 250ºC.

3.2. Solid phases

Thermodynamic properties of pure phases and solid solution end-members: The model reported in this contribution primarily focuses on the behavior of REE, U, and Th in phosphate solid
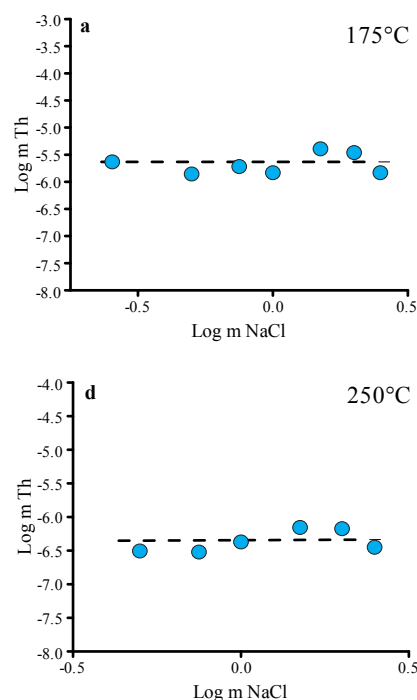
10

solutions and co-existing aqueous species. In addition, the model also needs to account for the coexisting uraninite (UO_2), U_3O_8 and U_4O_9 [37,38], thorianite (ThO_2 [49]), solid REE hydroxides[3], apatite-OH and whitlockite ($Ca_5(PO_4)_3OH$ and $Ca_3(PO4)_2$), halite (NaCl), hydrophilite ($CaCl_2$), and portlandite ($Ca(OH)_2$) [49]. Except for U and Th oxides, apatite-OH, and whitlockite, all other phases listed above were found unstable under the conditions employed in our model.

Thermodynamic properties of pure REE-phosphate end-members have been summarized in Migdisov et al. [3]. The data for *monazite end-members (LaPO₄ to GdPO₄)* were derived based on the calorimetric measurements by Navrotsky et al. and Popa et al. [50–52] and the values of solubility products determined for REE phosphates at 25 °C by Liu and Byrne [53]. The obtained dataset was tuned against the available solubility product of Nd-monazite endmember at temperatures up to 300 °C [54]. It was found that the derived dataset satisfactorily reproduces the high temperature solubility data [54]; it was however also found that higher temperature data reported by Pourtier et al. [55] drastically disagrees with both the derived thermodynamic properties of $NdPO_4$ and experimental determinations of its solubility product at lower temperatures (). Considering that the data reported in Pourtier et al. [55] do not agree with low-T determinations of the solubility product, calorimetric measurements, and experimental data reported in Poitrasson et al. [54], the data from Pourtier et al. [55] were
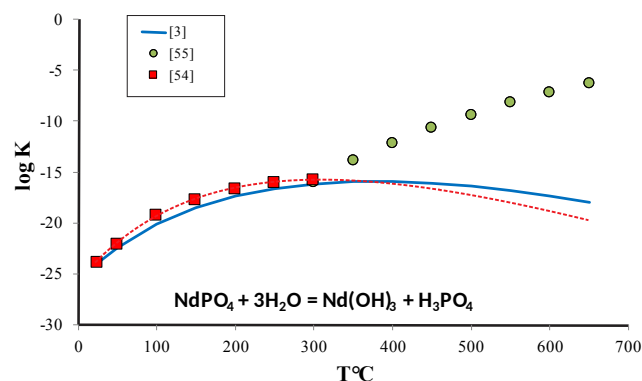

Figure 7. Comparison of the values of the dissolution equilibrium constant for Nd phosphate, re-calculated from the experimental data of Poitrasson et al. [54], calculated using the data summarized in [3], and experimentally determined by Pourtier et al. [55]

disregarded. Thermodynamic properties for *xenotime end-members (YPO₄, and TbPO₄ to LuPO₄)* were derived based on the calorimetric data reported in Navrotsky et al. and a set of studies of Gavrichev et al. [52,56–60], and, similarly to monazites, on the values of the solubility products reported for 25 °C [53]. The obtained dataset is in excellent agreement with the experimentally determined [61] solubility products of xenotimes at temperatures up to 250 °C (Figure 8).

The incorporation of actinides (U, Th) in monazites or xenotimes has been documented to occur via charge-couple ionic substitutions [7,62–66] (Fig. 1): the brabantitic (or cheralite, $Ca_{0.5}Th_{0.5}PO_4$) substitution (2) or the huttonite ($ThSiO_4$) substitution (3), as expressed below:

$$2REE^{3+} \leftrightarrow (U,Th)^{4+} + Ca^{2+} \tag{2}$$

$$REE^{3+} + P^{5+} \leftrightarrow (U,Th)^{4+} + Si^{4+} \tag{3}$$

The brabantitic substitution (2) occurs over the REE site while the huttonite substitution (3) occurs over both the REE and P tetrahedral sites. Because of the lack of experimental data related to substitution (3), our models focus on substitution (2), where the extra charge introduced by the tetravalent An is accommodated via incorporation of Ca^{2+} into the structure. It
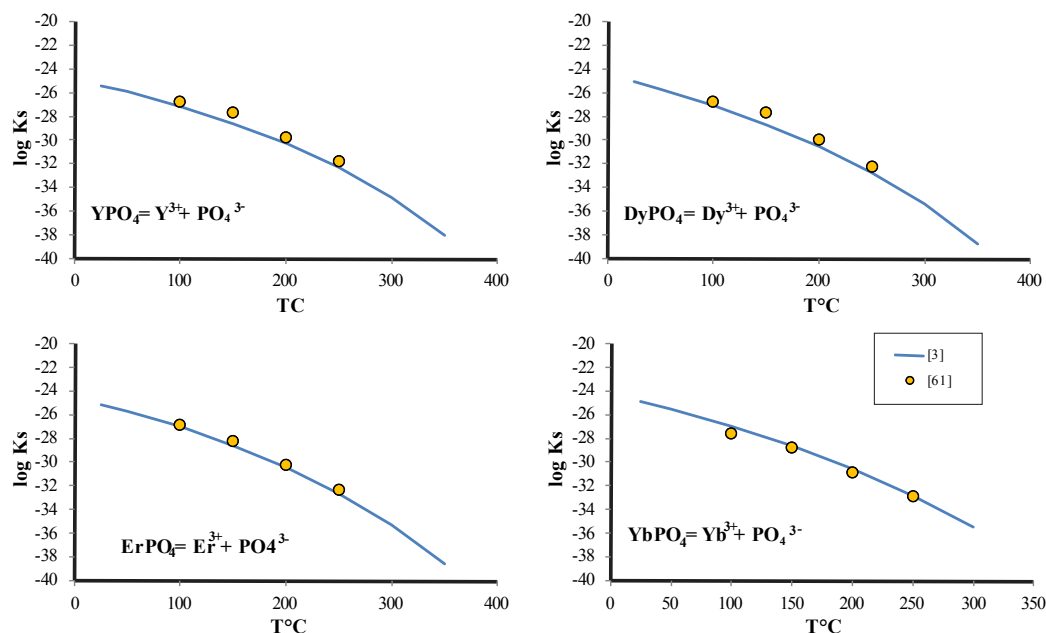
Figure 8. Comparison of the values of the solubility products for xenotime obtained experimentally by Gysi et al. [61], with those calculated based on the data summarized in [3]

should be pointed out that our inability to account for substitution (3) may lead to additional uncertainty associated with the trends described in our model. Thermodynamic properties of *pure (Ca, Th)PO₄ end-member* were taken from [67,68]. Information on the properties of *pure (Ca, U)PO₄ end-member* is much sparser and is restricted to the Gibbs free energy of formation determined by Muto [69] at 25 °C. Considering that the averaged mass of the (Ca, U) substituting pair is identical to that of La (139), to the first approximation, we assumed that the changes in $\Delta G°_f$ for (Ca, U)PO₄ with temperature, and, thus, the values of entropy and temperature dependence of heat capacity are identical to those for LaPO₄. Though reasonable, this is a rough approximation, thereby needing future verification.

Mixing properties of monazite and xenotime solid solutions: The mixing behavior of REE in the monazite and xenotime structures has been investigated from both experimental and computational perspectives. For solid solutions, depending on their free energy, enthalpy and entropy of mixing, they may form ideal solution, regular solution and subregular solution, the latter two of which require introduction of an interaction parameter to describe their mixing behavior.

To determine the mixing systematics of L/MREE in monazite and HREE in xenotime, we employed a regular solid solution model in which the excess enthalpy of mixing ΔH^E_{mix} is expressed as $W \cdot x(1-x)$, where W is the interaction parameter and x is the portion of one REE over the cation site. Calorimetric techniques have been used to determine W values of various solid

12

solution systems with good precisions, as demonstrated by previous high-temperature oxide-melt
drop-solution calorimetric studies of spinel, yttrium stabilized zirconia, silicates, titanates and
niobates [70–75]. However, only a few phosphate systems have been studied calorimetrically
with the exception of La-Ln(-An) phosphates [76–80], and thus there is a knowledge gap in
understanding the mixing behavior of REE monazite and xenotime solid solutions from
experimental data. Kowalski and Li [81], and Mogilevsky [82] tried to fill this gap using *ab
initio* calculations implemented with models linking the mixing energetics with lattice energy
strains; they proposed the main contributor to the excess mixing properties of two REE in
monazite to be the strain energy originated from the mismatch of these two different REE cations
in the nine-coordinated (monazite) or eight-coordinated (xenotime) sublattices. Specifically, the
Margules interaction parameters can be expressed as a function of the volume mismatch from the
two end-members and are proportional to the average Young's modulus $\overline{E}$:

$$W = \overline{E} \cdot (\Delta V^2 / 6V). \qquad (4)$$

For modelling the monazite system, we used interaction parameters (Table 2) that were obtained
from calorimetric measurements or from theoretical calculations [78,81] by Kowalski and Li
based on the available experimentally measured Young's moduli and molar volumes of end-
members. As for the xenotime system, the Young's moduli (E) and thus interaction parameters
(W) are largely unknown. Instead, Mogilevsky estimated E values of monazites and xenotimes
from the ionic radii R of the cations, and found a near linear correlation [82]. We assessed such
correlation with known and newly available elastic constants data [83–85] and plotted them in
Figure 9.

The new E_x-R_x function for xenotime is:

$$E_x = 1320.4(\pm179.6) - 1142.8(\pm178.0) \cdot R_x. \qquad (5)$$

From the R_x for all of HREE (Tb
→ Lu and Y), we calculated each
of their E_x based on equation (5).
The average Young's modulus
and molar volume for xenotimes
were calculated to be $\overline{E_x}$ = 168.8
GPa and $\overline{V_x}$ = 42.520 cm^3/mol.
Next, we determined W_x in terms
of ΔV, $\overline{E_x}$ and $\overline{V_x}$ based on
equation (4), plotted in Figure 10.
As demonstrated previously by
Glynn [86], in order for a solid-
solution system to be
thermodynamically stable, the
interaction parameter needs to be
constrained by $W/(K_B T) < 2$,
which translates to W < 5 kJ/mol
under the ambient condition. All
the calculated W_x values are well
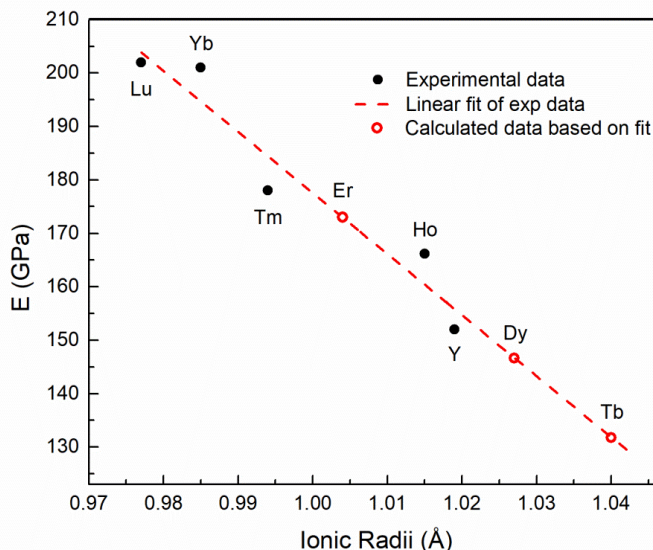below 5.0 kJ/mol, indicating that

Figure 9. The correlation of Young's moduli E_x with eight-coordinated ionic radii R_x in the xenotime matrix. A near linear relation (red dash curve) was revealed based on known experimental E_x data (black solid dots), which was used to calculate E_x (red circle) for other HREE.

13

there are no miscibility gaps for HREE solid-solutions in the xenotime structure. We evaluated the size of the pseudo cation (Ca,An) pair by averaging their eight-coordinated ionic radii, 1.085 and 1.060 Å, for (Ca,Th) and (Ca,U), respectively. Fitted by the function plotted in Figure 10, the calculated W_x values for (Ca,Th) and (Ca,U) are also listed in Table 3. Note that although the W_x values for (Ca,Th) and (Ca,U) are generally large, they could still be underestimated because, despite the average charge for the cation-pair being trivalent, each divalent Ca or tetravalent U/Th cation locally occupies an individual site, generating additional Coulombic interactions with its nearest (or next to the nearest) neighbors that could distort the sublattices, leading to an increase of the excess mixing enthalpy.

The most common monazites occurring in nature are monazite-(Ce) and monazite-(La). Monazite-(Nd) is also found in natural systems but is much rarer. Thus, in our model we accounted for two types of monazite: monazite-(Ce), containing $CePO_4$, $PrPO_4$, $NdPO_4$, $SmPO_4$, $GdPO_4$, $(Ca,Th)PO_4$, and $(Ca,U)PO_4$, and monazite-(La), containing $LaPO_4$, $PrPO_4$, $NdPO_4$, $SmPO_4$, $GdPO_4$, $(Ca,Th)PO_4$, and $(Ca,U)PO_4$. This separation into two types of monazites is necessary, also due to limitations of the software (HCh), which cannot account for solid solutions having more than 7 components. Formation of monazite-(Nd) was assumed when $NdPO_4$ was predominated in one of the above solid solutions. Xenotime was defined in the model as the solid solution containing YPO_4, $TbPO_4$, $DyPO_4$, $ErPO_4$, $YbPO_4$, $(Ca,Th)PO_4$, and $(Ca,U)PO_4$.
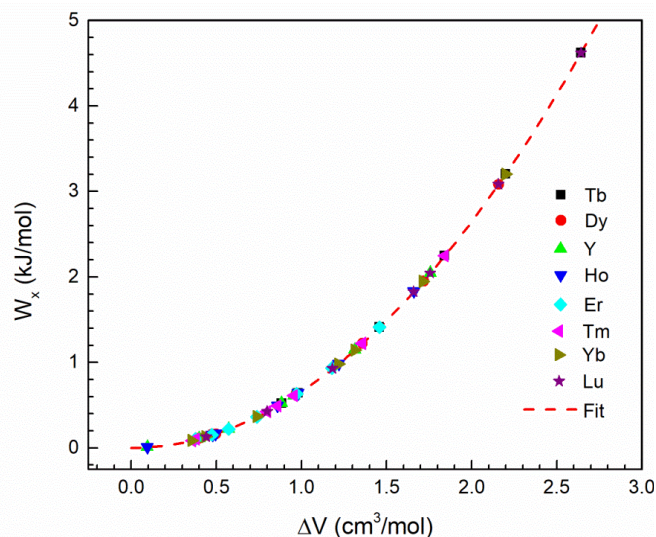

Figure 10. The fitted correlation between the interaction parameters W_x and the difference molar volume ΔV, with selected calculated points for HREE endmembers

4. Results

4.1. Aqueous speciation

The selected range of pH^T for the solutions in our calculations ($pH^T \leq 2$) reflects the conditions documented for Strange Lake, Canada, a natural ore forming system [17]. Our previous models [3,87] suggest that at these pH conditions and in NaCl-rich solutions, REE speciation is strictly predominated by chloride complexes. Differences in stability between LREE and HREE chloride complexes, which start developing as temperatures increase, is a main mechanism for natural REE separation.

As expected, speciation of the REE in our model was overwhelmingly predominated by chloride complexes. An example of the changes in species distribution with temperature at the initial stage of interaction of REE-bearing solution with apatite-bearing rock is shown in Figure 11 for Y, La, Nd, and Er (Y, LREE, MREE, and HREE, respectively). Regardless of a change in total

REE concentration at following interactive stages, the species distribution remains the same due to the constant concentration of chloride. The mass balance of REE dissolved in aqueous solution was primarily controlled by the bichloride complex, $REECl_2^+$, for LREE, the bichloride and monochloride complexes, $REECl_2^+$ and $REECl^{2+}$, respectively, for MREE, and by monochloride complexes for HREE. The only exception from this trend is Y whereby the data used in our calculation suggests that Y^{3+} contributes significantly to the mass balance of dissolved Y, being the predominant species at T<300 °C (Figure 11a). This could potentially be an artifact of our approximate evaluation of the properties of Y-chloride species. Thus, again we remind the readers that due to the complete absence of data on these species, we assumed identical properties to those of Ho-chloride complexes. Evidently, this assumption may eventually be erroneous and further refinement of the properties of Y-chloride complexes is needed.

Similarly to the REE, speciation of U was predominated by chloride complexes, while sulfate complexes did not contribute significantly to the mass balance of dissolved U, at both reducing and oxidizing conditions. Under reducing conditions the predominant U-bearing species is $UCl_4°$, whereas at oxidizing conditions most of the U is present as $UO_2Cl_2°$. Figure 12 illustrates the U species distribution returned by the model. Surprisingly, the stability of $UCl_4°$ was found to contribute significantly (10 -20%) to the mass balance of dissolved U, even under oxidizing conditions. Despite its counterintuitiveness, this finding is not entirely new: the high stability of $UCl_4°$ at elevated temperatures has previously been discussed in Timofeev et al. [36]. Similarly, under reducing conditions, $UO_2Cl_2°$ also contributes at low level to the mass balance of dissolved U. Concentrations of total dissolved U in reducing and oxidizing systems differ by ~2 orders of
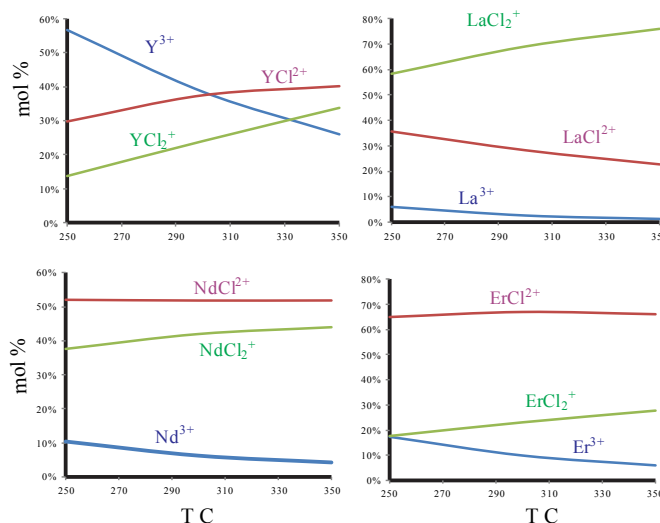

Figure 11. Distribution of predominant species of REE as a function of temperature (10 wt% NaCl)
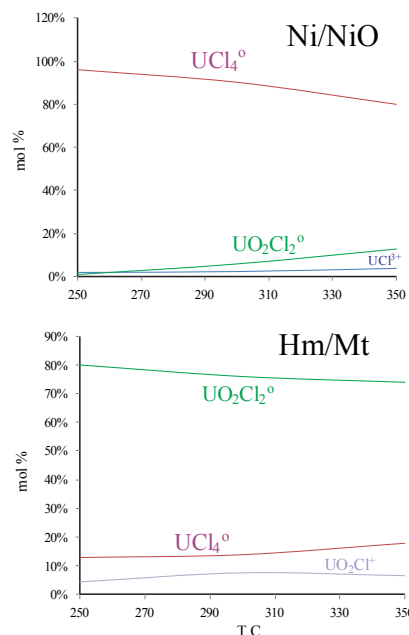

Figure 12. Distribution of predominant species of U as a function of temperature in 10 wt% NaCl solution in systems buffered by Ni/NiO redox buffer (a) and Hematite/Magnetite (Fe_2O_3/Fe_3O_4) redox buffer (b)

15

magnitude at 250 °C, while this difference reduces to one order of magnitude at 350 °C. Such small differences in total solubility of U are also due to the high stability of $UCl_4°$, as also discussed in Timofeev et al. [36]. Analogous to the REE, the distribution of U species remains consistent, while the total concentration of U changes when the fluid passes through the column — a result of continual high concentrations of NaCl in the solution.

Speciation of Th differs significantly from that of REE and U. The experiments reported by Nisbet et al. [40] did not reveal any contribution of Th chloride complexes in solutions with concentrations of NaCl up to 2.5 mol/kg and temperatures up to 250 °C. Thus, our model did not account for these species. The only complex controlling the solubility of Th was $Th(OH)_2^{2+}$. Considering that the mobility of Th in the modeled solutions is controlled by hydroxyl complexes, its species distribution must be pH-dependent. It should be noted that the pH^T values of the solutions passing through the column shifts from an 1.9-2.0 to 2.5-2.8 due to the buffering effect from the interaction of acidic fluid with apatite. These pH^T changes, however, are not significant enough to change the predominant Th complex in the solution, as the other hydroxyl species described to control the mobility of Th in NaCl-bearing solutions in Nisbet et al. [40], $Th(OH)_4°$, predominates only at $pH^T \geq 3$.

Examples of changes in total concentrations of dissolved metals along the column are shown in . The patterns obtained for REE are similar to those reported previously [3,87]. The initial depositional event, i.e., the first contact of the REE-bearing solution with rock containing excess apatite, causes quick deposition of effectively all the REE solution load in the form of highly insoluble xenotime and monazites. This continues until the apatite content in the rock is exhausted. The following aliquots of the REE-bearing solution re-equilibrates with previously deposited REE phosphates. Significantly higher stability of LREE chloride complexes, compared to the HREE complexes, leads to the preferential deposition of HREE phosphates at the expense of LREE phosphates:

Figure 13. Distribution of total concentrations of REE, U, and Th in aqueous solution observed in the model along the column

$$LREEPO_4^{solid} + HREECl^{2+} + Cl^- = HREEPO_4^{solid} + LREECl_2^+ \qquad (6)$$

As a result of this process, LREE become re-mobilized by the solution, and concentrations of these elements steadily increase along the altered part of the column, whereas the concentrations of HREE quickly decrease due to continuous deposition of solid HREE phosphates. In the case of La, this process manifests itself to an extreme pattern: as it can be seen from Figure 13, La
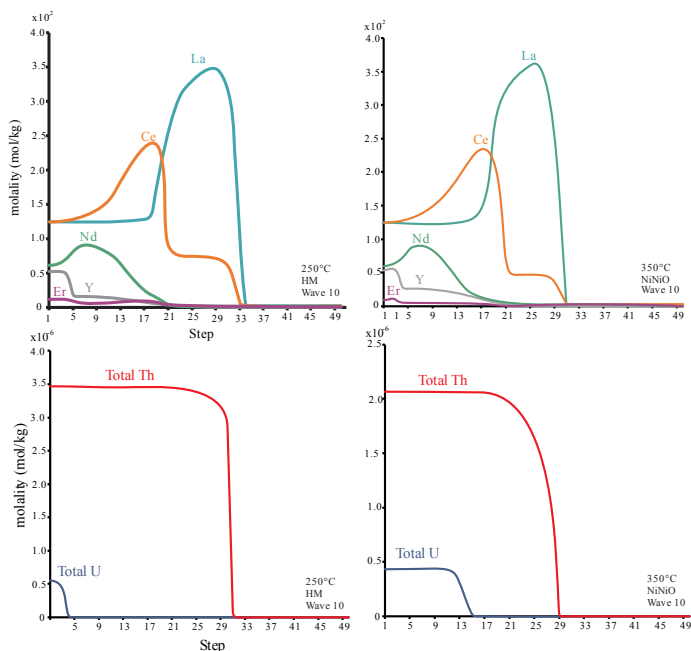
16

forms a concentration peak at the front of alteration. These distribution patterns of REE were observed at all temperatures in the conditions tested.

Surprisingly, although U is expected to behave in significantly different ways in reducing and oxidizing systems, the patterns observed for total concentrations of U are very similar for both types of systems. The U load in the solution quickly drops at the beginning of the column, reducing its concentration to insignificant levels. Continuous flushing of the system with U-bearing solution partially mobilizes U, however this happens with significant delay compared to other elements. This observed outcome can be described as solid solution-controlled, as further discussed next.

Due to the high stability of $Th(OH)_2^{2+}$ species, concentrations of Th initially developed in the solutions (re-equilibration with ThO_2^{solid}) are approximately one order of magnitude greater than that for U even at oxidizing conditions, but still 4 to 5 orders of magnitude lower than that developed by REE (Figure 13). Thorium concentration remains steady in altered, apatite-depleted rock, and begins decreasing near, and abruptly drops at the alteration front. This quick decrease at the alteration front is associated with two concordant processes: 1) the decrease of pH from 1.9 to ~2.5-2.7 due to interaction of acidic solution with apatite, which decreases the stability of $Th(OH)_2^{2+}$ in solutions saturated with respect to Th oxide, and 2) the incorporation of Th in solid solutions, which will be discussed below.

4.2. Solid solutions

Initial contact of the solutions with the apatite-bearing rock results in intensive precipitation of REE, U, and Th in the form of monazite and xenotime. Considering the near complete removal of REE, U, and Th from the solutions at the initial stage (excess of apatite), the initial ratio of REE, (Ca,U), and (Ca,Th) phosphates in monazite and xenotime solid solutions reflects the ratio of these elements in aqueous solutions, which was developed before interaction with the apatite-bearing rock.

Once the apatite is exhausted from the rock, continuous flushing of the deposited xenotime and monazite with REE-, U-, and Th-bearing fluid results in re-distribution of REE phosphates along the column. More mobile LREE, especially La and Ce, are re-mobilized in accordance to reaction (6). At elevated temperature, La chloride complexes demonstrate the highest stability among the REE chloride species (Figure 3). Thus, monazite-(La) quickly disappears from the beginning of the column, as it is mobilized by the solution closer to

Figure 14. Distribution of total amounts of monazites and xenotime (mol) re-deposited in the column at 250 ºC after 10 waves (flushes) in a system buffered with Hematite/Magnetite redox buffer.

the alteration front, forming a deposition peak (). Re-distribution of monazite-(Ce) lags behind monazite-(La), and forms a deposition peak before the monazite-(La) peak. As shown in Figure 14, after only a few flushes of the fluid through the column, the separation of monazite-(La) and
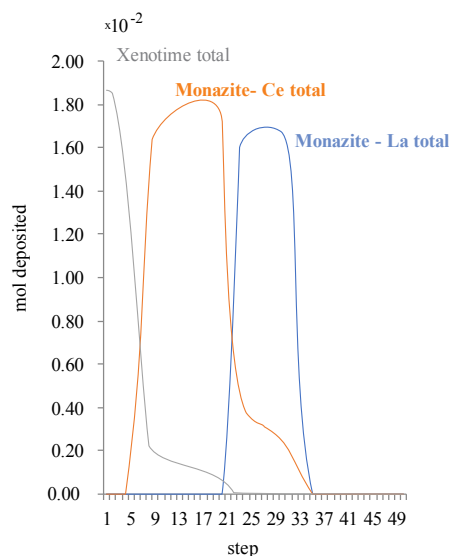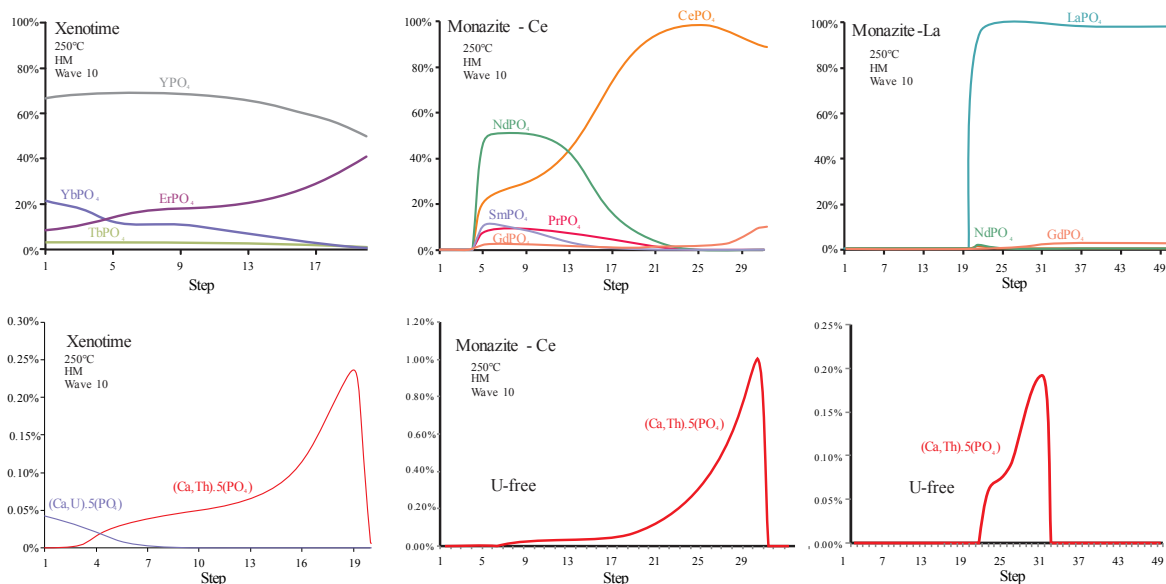
Figure 15. Concentrations of end-members in re-deposited REE phosphates (250 °C, HM, 10 waves)

monazite-(Ce) is nearly complete. Interestingly, whereas the content of the re-distributed monazite-(La) is 99 mol% LaPO₄, and this phase is highly depleted of other REE phosphate end-members, the composition of the re-distributed monazite-(Ce) varies significantly (Figure 15). Closer to the alteration front, the re-distributed monazite-(Ce) contains more than 99 mol% CePO₄, with only trace amounts of other phosphate end-members, mostly NdPO₄. However, at the tail of the monazite-(Ce) re-distribution peak, the content of NdPO₄ increases by up to 50 mol%, accompanied with an appreciable increase of other phosphate end-members (~10 mol% SmPO₄ and PrPO₄). The composition of monazite-(Ce) in this area of the column permits us to classify this phase as monazite-(Nd), the most industry-sought type of monazite. Monazite-(Ce) also co-deposits with monazite-(La) at ~20 mol% level (Figure 14). In this range, monazite-(Ce) becomes enriched with the GdPO₄ end-member; we do not exclude however that this can be an artifact of our simplistic description of solid solution and artificial separation of monazite to two phases due to restrictions of the applied software. A more complex model will likely include monazite-(Ce) co-deposited with monazite-(La) into the composition of the latter. At high temperatures, stability of HREE chloride complexes is lowest in the REE group of elements, and, thus, re-distribution of xenotime along the column is the least significant among the solid solutions considered in our model. The deposition of xenotime occurs at the beginning of the column, and while the solution flushes through the system, re-distributes it to the areas preceding that of re-distribution peak of monazite-(Ce). Compositions of re-distributed xenotime also follow the trend observed for monazites: depletion of lighter end member REE phosphates (ErPO₄, in the case of xenotime) at the beginning of the re-distribution peak, and its enrichment closer to the end of this peak. The model also suggests co-deposition of xenotime with monazite-(Ce) at ~5 mol% level. This, however, also could be an artifact of over-simplified solid solution models used in our calculations: a more complex model can potentially include the 5 mol% components of co-deposited xenotime into the composition of monazite.

18

Thus, our model shows that after 5 to 10 flushes of the solution through the system, complete separation of the REE phosphates: xenotime, monazite-(Nd), monazite-(Ce), and monazite-(La) was evident. The trends described above were observed for all temperatures evaluated in our model, and, considering our model only accounted for REE(III), REE was redox insensitive for all oxygen fugacities.

With excess REE in aqueous solution, Th deposits within both xenotime and monazite solid solutions. Its distribution along the column behaves similarly to that of REE: mobilization of Th from the beginning of the column and re-deposition closer to the alteration front. Combined with the separation of REE phosphates described above, re-distributed Th primarily occurs in monazite, while xenotime becomes depleted. The amount of $(Ca,Th)PO_4$ deposited along the column are shown on Figure 16; as seen in the figure the main mass of re-distributed Th is associated with the deposition of monazite. Our model therefore suggests that under the tested conditions, Th preferentially fractionates into monazite, which is consistent with the crystal-chemical argument described earlier.

In contrast to Th, U strictly and preferentially fractionates into to xenotime. With the exception of the initial depositional event (first encounter of unaltered solution with unaltered rock), at which U incorporates in both monazite and xenotime, U was not found in any re-distributed monazites, and all occurrence of $(Ca,U)PO_4$ end-member was associated with xenotime. Interestingly, although we tested significantly different redox conditions in our model, which should result in substantial differences in the mobility of U, the abovementioned trend remained the same. Thus, the model suggests very high stability of $(Ca,U)PO_4$ end-member in xenotime solid solution, whereby irrespective of total concentrations of U in solution and the oxidation state of this element, formation of xenotime effectively immobilizes all U available in solution, preventing its incorporation into the monazites. The amount of $(Ca,U)PO_4$ deposited along the column are shown in ; as it can be seen from the figure the main mass of re-distributed U is strictly associated with deposition of xenotime.
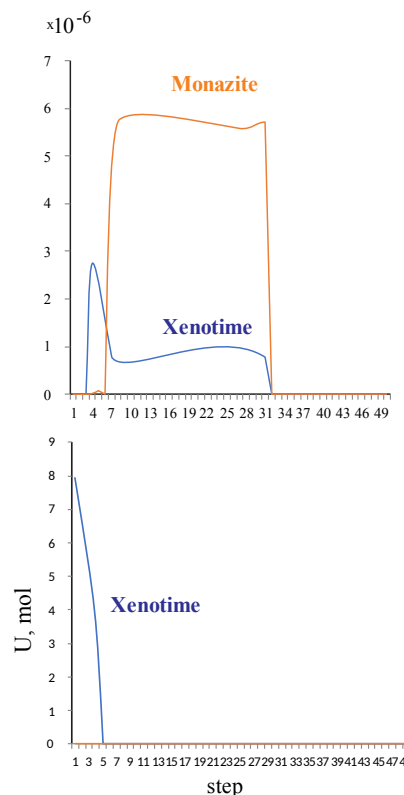

Figure 16. Total amounts of U and Th deposited with REE phosphates (250 °C, HM, 10 waves)

5. Discussion

The calculations reported in this contribution confirm the conclusions obtained in our earlier, more simplistic models [3,87]: deposition/re-distribution of REE phosphates from/by hydrothermal acidic NaCl-rich natural fluids can potentially lead to a very efficient separation of

705 xenotime from monazite. The main driving force of this separation is the increase in stability of chloride complexes of LREE, comparing to that of HREE, which occurs at elevated temperatures (Figure 3). Chloride complexes of the REE remain weak at elevated T, however this is overwhelmed by high concentrations of chloride in solutions responsible in nature for the transport and concentration of REE to economic levels. Deposition of xenotime and monazite
710 from aqueous solution requires a source of phosphate. In our calculations, which reflect the most likely scenario in nature, the source of phosphate is apatite or whitlockite ($Ca_5(PO_4)_3OH$ and $Ca_3(PO4)_2$) that are present in trace concentrations in the rock. The presence of these minerals in a rock through which REE-bearing aqueous solution flowed would form a geochemical barrier and initiate deposition of REE phosphates, e.g.:

715 $$Ca_5(PO_4)_3OH + 3REECl^{2+} + H^+ = 3REEPO_4 + 3CaCl^+ + 2Ca^{2+} + H_2O \qquad (7)$$
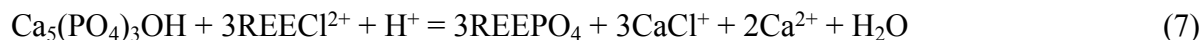
As it can be seen from equation (7), interaction of dissolved REE with apatite is an H^+ consuming reaction. Strictly speaking, this reaction is not a pH-buffering process, however, at given concentrations of apatite in the rock, its complete consumption through the formation of REE phosphates can be considered as an analogue of a pH-buffering process. The solubility of
720 REE phosphates is significantly lower than that of apatite (and most naturally occurring phosphates, Figure 17); thus, until apatite is present in the rock, the formation of REE phosphates occurs indiscriminately by removing effectively all REE load from the solution.

725 The observed separation of monazite and xenotime begins when all apatite content is exhausted (reaction 6). Flushing hydrothermal fluid through the
730 column depletes the already deposited REE phosphates with LREE, and re-mobilizes them to a new location, leaving HREE-enriched phases behind. This
735 suggests that the effects of this separation should be visible in well-

Figure 17. Solubility products of monazite/xenotime end members as a function of temperature

evolved hydrothermal systems, characterized by relatively high fluid/rock ratio, when REE-carrying capacity of a fluid exceeds binding capacity of a rock. In this case, xenotime should be found in the most evolved parts of the system, characterized by highest fluid/rock ratio, whereas
740 monazite can be found at the periphery of the system with lower fluid/rock ratios. Another scenario that can lead to a similar effect is the late alteration of already deposited REE phosphates by REE-free hydrothermal fluids. Although this scenario has not been evaluated in our model, it is evident that the processes occurring in such systems should be similar to that modeled in this contribution.

745 A critical reservation when discussing the results of our model is the behavior of Y in hydrothermal aqueous solutions. It should be recalled that due to a lack of any experimental or theoretical evaluation of the properties of Y chloride species at elevated temperatures, in the calculations reported above these properties were assumed to be identical to those of Ho chloride species. This assumption is highly approximate; accurate description of its behavior in NaCl-
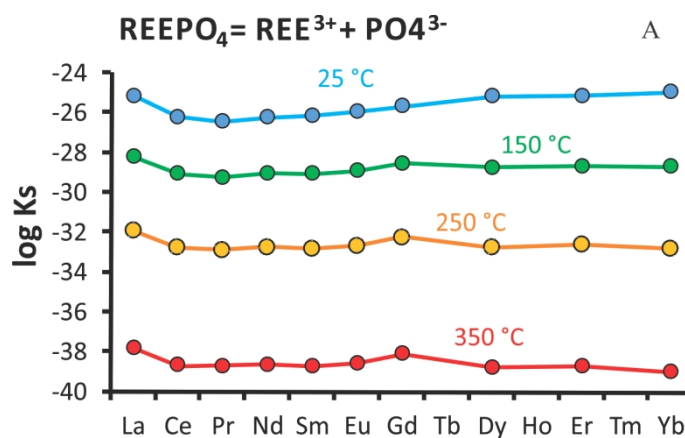
750   bearing solutions requires accumulation of experimental information. At the same time, Y is the main mineral-forming element in xenotime, and therefore potential inaccuracy in the description of its behavior in aqueous solution can cause deviations of the dependencies observed in our model from the true trends.

    A notable finding returned by our model is the behavior of U and Th during the processes of
755   hydrothermal deposition and fractionation of REE. Our model suggests Th preferentially fractionates into monazite, while U is strongly bound to xenotime. Indeed, this fractionation has been documented for natural monazites and xenotimes. For example, strong fractionation of Th and U into monazite and xenotime, respectively has been recorded in REE phosphates found in metapelites and granites in Germany [88,89]; extreme enrichment of Th versus U was found in
760   hydrothermally altered monazites in Swiss Alps [90]; and finally, a very similar effect of fractionation of U and Th has been documented for minerals growing during hydrothermal alteration at contact boundaries between granite and gabbro in the Unazuki region, Japan [90]. The above findings suggest that, although highly simplified, the model proposed in this contribution reproduces general trends observed in natural systems.

765   The opposing behavior of U and Th can be attributed to the differences in the REE polyhedral sites between the monazite and xenotime structure (Fig. 1). In the parent $CePO_4$ monazite structure, the ionic radius of Ce^{3+} in a nine-coordinated site is 1.196 Å. By contrast, in the parent YPO_4 xenotime structure, the ionic radius of Y^{4+} in an eight-coordinated site is 1.019 Å [9]. Thus, it is not surprising that the larger M/LREE favors the monazite structure the smaller HREE
770   prefers the xenotime structure. Since Th is larger than U (the ionic radii of Th^{4+} and U^{4+} in an eightfold coordination are 1.09 Å and 1.05 Å), Th favors the more expanded monazite structure and U favors the denser xenotime structure. This situation is even truer with the concomitant incorporation of the larger Ca^{2+} (the ionic radii of Ca^{2+} in an eightfold and ninefold coordination are 1.12 Å and 1.18 Å, respectively) into either structure to achieve charge neutrality, especially
775   when the concentration of Ca+U or Ca+Th is relatively low.

    The model reported in this contribution, unfortunately, does not propose any mechanisms for formation of U- or Th-free monazites or xenotimes. Presence of actinides in aqueous solutions inevitably leads to the formation of either U-containing xenotimes, or Th-containing monazites, irrespective of the degree of alteration. We note, however, that in systems of different chemistry
780   (e.g., systems with sulfate- or carbonate-ligands), U or Th complexes potentially might be more stable (and, thus, more mobile) than those accounted for in our calculations, and there is still potential possibility that the Th-free monazites can be formed due to higher mobilization capacity of the fluids.

6. Conclusions

785   The model reported in this contribution confirms our preliminary conclusions [3,87] and demonstrates that the interaction of REE phosphates with NaCl-rich acidic fluid can lead to the complete separation of xenotimes that are rich in M/LREE from monazites that are rich in HREE. This separation is accompanied by preferential fractionation of U to xenotime and Th to monazite. Both monazite/xenotime separation and U/Th fractionation are consistent with the
790   crystal-chemical argument on the differences between the two parent structures in the context of substituting ionic size effect. This phenomenon is known from natural observations and has been documented for a number of naturally occurring monazites and xenotimes.

800   **7.   References**

[1]   R. U.S. Department of Energy, U.S. Department of Energy. Critical Materials Strategy,
        Washington, D.C., 2011.

[2]   R. U.S. Geological Survey, U.S. Geological Survey: Mineral Commodity Summaries
805   2017, Reston, Virginia, 2017.
        https://minerals.usgs.gov/minerals/pubs/mcs/2017/mcs2017.pdf.

[3]   A. Migdisov, A.E. Williams-Jones, J. Brugger, F.A. Caporuscio, Hydrothermal transport,
        deposition, and fractionation of the REE: Experimental data and thermodynamic
        calculations, Chem. Geol. 439 (2016) 13–42. doi:10.1016/j.chemgeo.2016.06.005.

810   [4]   D. Banks, B. Yardley, A. Campbell, K. Jarvis, REE composition of an aqueous magmatic
        fluid: A fluid inclusion study from the Capitan Pluton, New Mexico, U.S.A., Chem. Geol.
        113 (1994) 259–272. doi:10.1016/0009-2541(94)90070-1.

[5]   R. Gratz, W. Heinrich, Monazite-xenotime thermobarometry: Experimental calibration of
        the miscibility gap in the binary system CePO4-YPO4., Am. Mineral. 82 (1997) 772–780.

815   [6]   Y. Ni, J.M. Hughes, A.N. Mariano, Crystal chemistry of the monazite and xenotime
        structures, Am. Mineral. 80 (1995) 21–26.

[7]   M. Cuney, M. Friedrich, Physicochemical and crystal-chemical controls on accessory
        mineral paragenesis in granitoids: implications for uranium metallogenesis, B Miner. 110
        (1987) 235–247.

820   [8]   E.R. Vance, Y. Zhang, T. McLeod, J. Davis, Actinide valences in xenotime and monazite,
        J. Nucl. Mater. 409 (2011) 221–224.

[9]   R.D. Shannon, Revised effective ionic radii and systematic studies of interatomic
        distances in halides and chalcogenides, Acta Crystallogr. A32 (1976) 751–767.

[10]   T. Ault, B. Van Gosen, S. Krahn, A. Croff, Natural Thorium Resources and Recovery :
825   Options and Impacts, Nucl. Technol. 194 (2016) 136–151.

[11]   C. Sonich-Mullin, Rare Earth Elements : A Review of Production , Processing , Recycling
        , and Associated Environmental Issues Rare Earth Elements : A Review of Production ,
        Processing , Recycling , and Associated Environmental Issues, Washington, D.C., 2012.

[12]   M. Findeiß, A. Schaffer, Fate and Environmental Impact of Thorium Residues During
830   Rare Earth Processing, J.Sustain. Met. (2016). doi:10.1007/s40831-016-0083-3.

[13]   Y. Shvarov, E. Bastrakov, HCh: A Software Package for Geochemical Equilibrium
        Modeling – User's Guide., Aust. Geol. Surv. Organ. Rec. 1999. 25 (1999) 61.

[14]   M. Smith, P. Henderson, Preliminary fluid inclusion constraints on fluid evolution in the
        Bayan Obo Fe-REE-Nb deposit, Inner Mongolia, China, Econ. Geol. 95 (2000) 1371.
835   doi:10.2113/95.7.1371.

[15]   A.E. Williams-Jones, I.M. Samson, G.R. Olivo, The genesis of hydrothermal fluorite-REE
        deposits in the Gallinas Mountains, New Mexico, Econ. Geol. 95 (2000) 327–341.

[16]   B. Lehmann, S. Nakai, A. Höhndorf, J. Brinckmann, P. Dulski, U. Hein, A. Masuda, REE

840   mineralization at Gakara, Burundi: Evidence for anomalous upper mantle in the western Rift Valley, Geochim. Cosmochim. Acta. 58 (1994) 985–992.

[17]   A.P. Gysi, A.E. Williams-Jones, Hydrothermal mobilization of pegmatite-hosted REE and Zr at Strange Lake, Canada: A reaction path model, Geochim. Cosmochim. Acta. 122 (2013) 324–352. doi:10.1016/j.gca.2013.08.031.

[18]   J. Kestin, J. Sengers, B. Kamgar-Parsi, Thermophysical Properties of Fluid H20, J. Phys.
845   Chem. Ref. 13 (1984) 175–183. http://potomac.nist.gov/srd/PDFfiles/jpcrd250.pdf (accessed July 14, 2010).

[19]   W.L. Marshall, E.U. Franck, Ion Product of Water Substance, 0-1000°C, 1-10,000 Bars. New International Formulation and Its Background, J. Phys. Chem. Ref. Data. 10 (1981) 295–304.

850 [20]   E. Oelkers, H.C. Helgeson, Calculation of activity coefficients and degrees of formation of neutral ion pairs in supercritical electrolyte solutions, Geochim. Cosmochim. Acta. 55 (1991) 1235–1251. doi:10.1016/0016-7037(91)90303-M.

[21]   E. Oelkers, H.C. Helgeson, Triple-ion anions and polynuclear complexing in supercritical electrolyte solutions, Geochim. Cosmochim. Acta. 54 (1990) 727–738. doi:10.1016/0016-
855   7037(90)90368-U.

[22]   J.W. Johnson, E.H. Oelkers, H.C. Helgeson, SUPCRT92: A software package for calculating the standard molal thermodynamic properties of minerals, gases, aqueous species, and reactions from 1 to 5000 bar and 0 to 1000 °C, Comput. Geosci. 18 (1992) 899–947. doi:10.1016/0098-3004(92)90029-Q.

860 [23]   E.L. Shock, D.C. Sassani, M. Willis, D.A. Sverjensky, Inorganic species in geologic fluids: correlations among standard molal thermodynamic properties of aqueous ions and hydroxide complexes., Geochim. Cosmochim. Acta. 61 (1997) 907–50. http://www.ncbi.nlm.nih.gov/pubmed/11541225.

[24]   D. Sverjensky, E.L. Shock, H.C. Helgeson, Prediction of the thermodynamic properties of
865   aqueous metal complexes to 1000 C and 5 kb, Geochim. Cosmochim. Acta. 61 (1997) 1359–1412. doi:10.1016/S0016-7037(97)00009-4.

[25]   B.R. Tagirov, A. Zotov, N. Akinfiev, Experimental study of dissociation of HCl from 350 to 500° C and from 500 to 2500 bars: Thermodynamic properties of HCl°(aq), Geochim. Cosmochim. Acta. 61 (1997) 4267–4280. doi:10.1016/S0016-7037(97)00274-3.

870 [26]   P.C. Ho, D.A. Palmer, M.S. Gruszkiewicz, Conductivity Measurements of Dilute Aqueous HCl Solutions to High Temperatures and Pressures Using a Flow-Through Cell, J. Phys. Chem. B. 105 (2001) 1260–1266.

[27]   T. Holland, R. Powell, An internally consistent thermodynamic data set for phases of petrological interest, J. Metamorph. Geol. 16 (1998) 309–343.
875   http://www3.interscience.wiley.com/journal/119118597/abstract (accessed January 29, 2011).

[28]   E.L. Shock, D.C. Sassani, H. Betz, Uranium in geologic fluids: Estimates of standard partial molal properties, oxidation potentials, and hydrolysis constants at high temperatures and pressures, Geochim. Cosmochim. Acta. 61 (1997) 4245–4266.
880   doi:10.1016/S0016-7037(97)00240-8.

[29]   J. Haas, E.L. Shock, D. Sassani, Rare earth elements in hydrothermal systems: estimates of standard partial molal thermodynamic properties of aqueous complexes of the rare earth elements at high, Geochim. Cosmochim. Acta. 59 (1995) 4329–4350. doi:10.1016/0016-7037(95)00314-P.

885   [30]   S. Wood, D. Palmer, D. Wesolowski, P. Bénézeth, The aqueous geochemistry of the rare earth elements and yttrium. Part XI. The solubility of Nd (OH) 3 and hydrolysis of Nd3+ from 30 to 290 C at saturated water vapor pressure with in-situ pHm measurement, in: R. Hellmann, S.A. Wood (Eds.), Water-Rock Interact. Ore Depos. Environ. Geochemistry A Tribut. to David A. Crerar, 2002: pp. 229–256. doi:10.1016/0009-2541(90)90080-Q.

890   [31]   Y. Luo, R.H. Byrne, Yttrium and rare earth element complexation by chloride ions at 25 C, J. Solution Chem. 30 (2001) 837–845. http://www.springerlink.com/index/Q332187111792NJM.pdf (accessed November 18, 2011).

   [32]   M. Altmaier, E. Yalçıntaş, X. Gaona, V. Neck, R. Müller, M. Schlieker, T. Fanghänel,
895   Solubility of U(VI) in chloride solutions. I. The stable oxides/hydroxides in NaCl systems, solubility products, hydrolysis constants and SIT coefficients, J. Chem. Thermodyn. 114 (2017) 2–13. doi:10.1016/j.jct.2017.05.039.

   [33]   P. Wang, A. Anderko, J.J. Kosinski, R.D. Springer, M.M. Lencka, Modeling Speciation and Solubility in Aqueous Systems Containing U(IV, VI), Np(IV, V, VI), Pu(III, IV, V,
900   VI), Am(III), and Cm(III), Springer US, 2017. doi:10.1007/s10953-017-0587-x.

   [34]   Y. Xing, Y. Mei, B. Etschmann, W. Liu, J. Brugger, Uranium transport in F-Cl-bearing fluids and hydrothermal upgrading of U-Cu ores in IOCG deposits, Geofluids. (2018) in press.

   [35]   G.A. Parks, D.C. Pohl, Hydrothermal solubility of uraninite, Geochim. Cosmochim. Acta.
905   52 (1988) 863–875.

   [36]   A. Timofeev, A.A. Migdisov, A.E. Williams-Jones, R. Roback, A.T. Nelson, H. Xu, Uranium transport in acidic brines under reducing conditions, Nat. Commun. 9 (2018) 1– 7. doi:10.1038/s41467-018-03564-7.

   [37]   I. Grenthe, J. Fuger, R.J.M. Konings, R.J. Lemire, A.B. Muller, C. Nguyen-Trung,
910   CHEMICAL THERMODYNAMICS OF URANIUM, OECD Nuclear Energy Agency, Data Bank, Issy-les-Moulineaux (France), 1992.

   [38]   R. Guillaumont, T. Fanghänel, J. Fuger, I. Grenthe, V. Neck, D.A. Palmer, M.H. Rand, Update on the chemical thermodynamics of uranium, neptunium, plutonium, americium and technetium., 2003.

915   [39]   B.N. Ryzhenko, O. V. Bryzgalin, I.Y. Artamkina, M.Y. Spasennykh, A.I. Shapkin, An electrostatic model for the electrolytic dissociation of inorganic substances dissolved in water., Geochem. Int. 22 (1985) 138–144.

   [40]   H. Nisbet, A. Migdisov, H. Xu, X. Guo, V. van Hinsberg, A.E. Williams-Jones, H. Boukhalfa, R. Roback, An experimental study of the solubility and speciation of thorium
920   in chloride-bearing aqueous solutions at temperatures up to 250 °C., Geochim. Cosmochim. Acta, Press. (n.d.).

   [41]   A.A. Migdisov, H. Boukhalfa, A. Timofeev, W. Runde, R. Roback, A.E. Williams-Jones, A spectroscopic study of uranyl speciation in chloride-bearing solutions at temperatures up to 250 °C, Geochim. Cosmochim. Acta. 222 (2018) 130–145.
925   doi:10.1016/j.gca.2017.10.016.

   [42]   M. Dargent, J. Dubessy, L. Truche, E.F. Bazarkina, C. Nguyen-Trung, P. Robert, Experimental study of uranyl(VI) chloride complex formation in acidic LiCl aqueous solutions under hydrothermal conditions (T = 21 C–350 °C, Psat) using Raman spectroscopy, Eur. J. Mineral. 25 (2013) 765–775. doi:10.1127/0935-1221/2013/0025-
930   2319.

24

[43] A.A. Migdisov, W. Runde, A.E. Williams-Jones, H. Boukhalfa, R. Roback, A. Timofeev, Response to the comment "Uranyl-chloride speciation and uranium transport in hydrothermal brines: Comment on Migdisov et al. (2018)" by Dargent et al., Geochim. Cosmochim. Acta. 235 (2018) 509–512. doi:10.1016/j.gca.2018.06.015.

935 [44] M.H. Rand, F.J. Mompean, J. Perrone, M. Illemassene, Chemical Thermodynamics of Thorium, OECD, NEA, 2008.

[45] P.L. Zanonato, P.D. Bernardo, Z. Zhang, Y. Gong, G. Tian, J.K. Gibson, L. Rao, Hydrolysis of thorium(IV) at variable temperatures, Dalt. Trans. 45 (2016) 12763–12771.

[46] V. Neck, J.I. Kim, Solubility and hydrolysis of tetravalent actinides, Radiochim. Acta. 91 940 (2003) 253–262.

[47] D. Rai, A.R. Felmy, S.M. Sterner, D.A. Moore, M.J. Mason, The Solubility of Th(IV) and U(IV) Hydrous Oxides in Concentrated NaCl and MgCl Solutions, Radiochim. Acta. 79 (1997) 239–247.

[48] I. Grenthe, B. Lagerman, Studies on metal carbonate equilibria: 23. Complex formation in 945 the Th(IV)-H2O-CO2(g) system, Acta Chem. Scand. 45 (1991) 231–238.

[49] R.A. Robie, B.S. Hemingway, Thermodynamic properties of minerals and related substances at 298.15 K and 1 Bar (105 Pascals) pressure and at higher temperatures., U. S. Geol. Surv. Bull. 2131 (1995) 461.

[50] K. Popa, D. Sedmidubsky, O. Benes, C. Thiriet, R. Konings, The high-temperature heat 950 capacity of LnPO4 (Ln=La, Ce, Gd) by drop calorimetry, J. Chem. Thermodyn. 38 (2006) 825–829. doi:10.1016/j.jct.2005.08.019.

[51] K. Popa, R.J.M. Konings, High-temperature heat capacities of EuPO4 and SmPO4 synthetic monazites, Thermochim. Acta. 445 (2006) 49–52. doi:10.1016/j.tca.2006.03.023.

955 [52] A. Navrotsky, W. Lee, A. Mielewczyk-Gryn, S. V. Ushakov, A. Anderko, H. Wu, R.C. Riman, Thermodynamics of Solid Phases Containing Rare Earth Oxides, J. Chem. Thermodyn. 88 (2015) 126–141. doi:10.1016/j.jct.2015.04.008.

[53] X. Liu, R.H. Byrne, Rare earth and yttrium phosphate solubilities in aqueous solution, Geochim. Cosmochim. Acta. 61 (1997) 1625–1633. doi:10.1016/S0016-7037(97)00037-9.

960 [54] F. Poitrasson, E. Oelkers, J. Schott, J.-M. Montel, Experimental determination of synthetic NdPO4 monazite end-member solubility in water from 21°C to 300°C: implications for rare earth element mobility in crustal fluids, Geochim. Cosmochim. Acta. 68 (2004) 2207–2221. doi:10.1016/j.gca.2003.12.010.

[55] E. Pourtier, J.-L. Devidal, F. Gibert, Solubility measurements of synthetic neodymium 965 monazite as a function of temperature at 2kbars, and aqueous neodymium speciation in equilibrium with monazite, Geochim. Cosmochim. Acta. 74 (2010) 1872–1891. doi:10.1016/j.gca.2009.12.023.

[56] K.S. Gavrichev, M. a. Ryumin, a. V. Tyurin, V.M. Gurevich, L.N. Komissarova, Heat capacity and thermodynamic functions of xenotime YPO4(c) at 0–1600 K, Geochemistry 970 Int. 48 (2010) 932–939. doi:10.1134/S0016702910090065.

[57] K.S. Gavrichev, M. a. Ryumin, a. V. Tyurin, V.M. Gurevich, a. V. Khoroshilov, L.N. Komissarova, Thermodynamic functions of erbium orthophosphate ErPO4 in the temperature range of 0–1600K, Thermochim. Acta. 535 (2012) 1–7. doi:10.1016/j.tca.2012.02.002.

975 [58] K.S. Gavrichev, N.N. Smirnova, V.M. Gurevich, V.P. Danilov, a. V. Tyurin, M. a. Ryumin, L.N. Komissarova, Heat capacity and thermodynamic functions of LuPO4 in the

25

range 0–320K, Thermochim. Acta. 448 (2006) 63–65. doi:10.1016/j.tca.2006.05.019.

[59] K.S. Gavrichev, M. a. Ryumin, a. V. Tyurin, V.M. Gurevich, G.E. Nikiforova, L.N. Komissarova, Heat capacity and thermodynamic functions of YbPO4 from 0 to 1800 K, Inorg. Mater. 49 (2013) 701–708. doi:10.1134/S0020168513070042.

[60] K.S. Gavrichev, M.A. Ryumin, A.V. Khoroshilov, G.E. Nikiforova, A.V. Tyurin, V.M. Gurevich, R.V. Starykh, Thermodynamic properties and phase transitions of tetragonal modification of terbium orthophosphate, Vestn. St.Petersbg. State Univ. 4 (2013) 186–197.

[61] A.P. Gysi, A.E. Williams-Jones, D. Harlov, The solubility of xenotime-(Y) and other HREE phosphates (DyPO4, ErPO4 and YbPO4) in aqueous solutions from 100 to 250°C and psat, Chem. Geol. 401 (2015) 83–95. doi:10.1016/j.chemgeo.2015.02.023.

[62] J. Finney, N.N. Rao, The crystal structure of cheralite, Am. Mineral. J. Earth Planet. Mater. 52 (1967) 13–19.

[63] H.-J. Forster, The chemical composition of REE-Y-Th-U-rich accessory minerals in peraluminous granites of the Erzgebirge-Fichtelgebirge region, Germany, Part I: The monazite-(Ce)-brabantite solid solution series, Am. Mineral. 83 (1998) 259–272.

[64] J. Hughes, E. Foord, M. Hubbard, Y. Ni, The Crystal-Structure Of Cheralite-(Ce),(LREE, Ca, Th, U)(P, Si) O-4, A Monazite-Group Mineral, Neues Jahrb. Fur Mineral. 8 (1995) 344–350.

[65] A.-M. Seydoux-Guillaume, R. Wirth, W. Heinrich, J.-M. Montel, Experimental determination of thorium partitioning between monazite and xenotime using analytical electron microscopy and X-ray diffraction Rietveld analysis., Eur. J. Mineral. 14 (2002) 869–878.

[66] H.J. Forster, Composition and origin of intermediate solid solutions in the system thorite-xenotime-zircon-coffinite, Lithos. 88 (2006) 35–55.

[67] K. Popa, T. Shvareva, L. Mazeina, E. Colineau, F. Wastin, R.J.M. Konings, a. Navrotsky, Thermodynamic properties of CaTh(PO4)2 synthetic cheralite, Am. Mineral. 93 (2008) 1356–1362. doi:10.2138/am.2008.2794.

[68] D. Rawat, S. Phapale, R. Mishra, S. Dash, Thermodynamic studies on charge-coupled substituted synthetic monazite, J. Nucl. Mater. 847 (2017) 406–417.

[69] T. Muto, Thermochemical stability of ningyoite, Mineral. J. 4 (1965) 245–274.

[70] X.F. Guo, S. Szenknect, A. Mesbah, N. Clavier, C. Poinssot, D. Wu, H.W. Xu, N. Dacheux, R.C. Ewing, A. Navrotsky, Energetics of a Uranothorite (Th1-xUxSiO4) Solid Solution, Chem Mater. 28 (2016) 7117–7124.

[71] H. Xu, A. Navrotsky, M.L. Balmer, Y. Su, Perovskite solid solutions along the NaNbO3-SrTiO3 join: Phase transitions, formation enthalpies, and implications for general perovskite energetics., Chem. Mater. 17 (2005) 1880–1886.

[72] H. Xu, P.J. Heaney, G. Beall, Phase transitions induced by solid solution in stuffed derivatives of quartz: A powder synchrotron XRD study of the LiAlSiO4-SiO2 join, Am. Mineral. 85 (2000) 971–979.

[73] H. Xu, Y. Su, M. Balmer, A. Navrotsky, A New Series of Oxygen-Deficient Perovskites in the NaTixNb1-xO3-0.5x System: Synthesis, Crystal Chemistry, and Energetics, Chem. Mater. 15 (2003) 1872–1878.

[74] H. Xu, A. Navrotsky, M.L. Balmer, Y. Su, E.R. Bitten, Energetics of substituted pollucites along the CsAlSi2O6-CsTiSi2O6.5 join: A high-temperature calorimetric study, J. Am. Ceram. Soc. 84 (2001) 555–560.

26

[75]   H. Xu, A. Navrotsky, M. Nyman, T. Nenoff, Octahedral microporous phases Na2Nb2−xTixO6−x(OH)x•H2O and their related perovskites: Crystal chemistry, energetics, and stability relations, J. Mater. Res. 20 (2005) 618–627.

[76]   K. Popa, R.J.M. Konings, T. Geisler, High-temperature calorimetry of (La1−xLnx)PO4 solid solutions, J. Chem. Thermodyn. 39 (2007) 236–239. doi:10.1016/j.jct.2006.07.010.

[77]   R.J.M. Konings, M. Walter, K. Popa, Excess properties of the (Ln2−2xCaxThx)(PO4)2 (Ln=La, Ce) solid solutions, J. Chem. Thermodyn. 40 (2008) 1305–1308. doi:10.1016/j.jct.2008.03.009.

[78]   Y. Li, P.M. Kowalski, A. Blanca-Romero, V. Vinograd, D. Bosbach, Ab initio calculation of excess properties of La1-x(Ln,An)(x)PO4 solid solutions, J Solid State Chem. 220 (2014) 137–141.

[79]   J.D. Bauer, A. Hirsch, L. Bayarjargal, L. Peters, G. Roth, B. Winkler, Schottky contribution to the heat capacity of monazite type (La,Pr)PO4 from low temperature calorimetry and fluorescence measurements, Chem Phys Lett. 654 (2016) 97–102.

[80]   A. Hirsch, P. Kegler, I. Alencar, J. Ruiz-Fuertes, A. Shelyug, L. Peters, C. Schreinemachers, A. Neumann, S. Neumeier, H.P. Liermann, A. Navrotsky, G. Roth, Structural, vibrational, and thermochemical properties of the monazite-type solid solution La1-xPrxPO4, J Solid State Chem. 245 (2017) 82–88.

[81]   P.M. Kowalski, Y. Li, Relationship between the thermodynamic excess properties of mixing and the elastic moduli in the monazite-type ceramics, J Eur Ceram Soc. 36 (2016) 2093–2096.

[82]   P. Mogilevsky, On the miscibility gap in monazite-xenotime systems, Phys Chem Min. 34 (2007) 201–214.

[83]   J.G. Berryman, Bounds and self-consistent estimates for elastic constants of random polycrystals with hexagonal, trigonal, and tetragonal symmetries, J Mech Phys Solids. 53 (2005) 2141–2173.

[84]   P. Mogilevsky, E.B. Zaretsky, T.A. Parthasarathy, F. Meisenkothen, Composition, lattice parameters, and room temperature elastic constants of natural single crystal xenotime from Novo Horizonte, Phys Chem Min. 33 (2006) 691–698.

[85]   O. Gomis, B. Lavina, P. Rodriguez-Hernandez, A. Munoz, R. Errandonea, D. Errandonea, M. Bettinelli, High-pressure structural, elastic, and thermodynamic properties of zircon-type HoPO4 and TmPO4, J Phys-Condens Mat. 29 (2017).

[86]   P. Glynn, Solid-solution solubilities and thermodynamics: sulfates, carbonates and halides, Rev. Mineral. Geochemistry. 40 (2000) 481–511.

[87]   A.A. Migdisov, A.E. Williams-Jones, Hydrothermal transport and deposition of the Rare Earth Elements by fluorine-bearing aqueous liquids, Miner. Depos. 49 (2014) 987–997.

[88]   G. Franz, G. Andrehs, D. Rhede, Crystal chemistry of monazite and xenotime from Saxothuringian-Moldanubian metapelites , NE Bavaria , Germany, Eur. J. Mineral. 8 (1996) 1097–1118. doi:10.1127/ejm/8/5/1097.

[89]   H. Forster, The chemical composition of REE-Y-Th-U-rich minerals in peraluminous accessory granites of the Erzgebirge-Fichtelgebirge Part II : Xenotime region , Germany ., Am. Mineral. 83 (1998) 1302–1315. doi:10.2138/am-1998-3-409.

[90]   E. Janots, A. Berger, E. Gnos, M. Whitehouse, E. Lewin, T. Pettke, Constraints on fluid evolution during metamorphism from U–Th–Pb systematics in Alpine hydrothermal monazite, Chem. Geol. 326–327 (2012) 61–71. doi:https://doi.org/10.1016/j.chemgeo.2012.07.014.

[91]   C.H. Gammons, S.A. Wood, A.E. Williams-Jones, The aqueous geochemistry of the rare
1070   earth elements and yttrium: VI. Stability of neodymium chloride complexes from 25 to
                   300°C, Geochim. Cosmochim. Acta. 60 (1996) 4615–4630. doi:10.1016/S0016-
                   7037(96)00262-1.

[92]   S. Stepanchikova, G. Kolonin, Spectrophotometric study of Nd, Sm, and Ho complexation
                   in chloride solutions at 100–250 C, Russ. J. Coord. 31 (2005) 193–202.
1075   doi:10.1007/s11173-005-0076-4.

[93]   A.A. Migdisov, A.E. Williams-Jones, A spectrophotometric study of neodymium (III)
                   complexation in chloride solutions, Geochim. Cosmochim. Acta. 66 (2002) 4311–4323.
                   doi:10.1016/S0016-7037(02)00995-X.

[94]   A.A. Migdisov, A.E. Williams-Jones, A spectrophotometric study of erbium (III)
1080   speciation in chloride solutions at elevated temperatures, Chem. Geol. 234 (2006) 17–27.
                   doi:10.1016/j.chemgeo.2006.04.002.

[95]   A.A. Migdisov, A.E. Williams-Jones, C. Normand, S.A. Wood, A spectrophotometric
                   study of samarium (III) speciation in chloride solutions at elevated temperatures,
                   Geochim. Cosmochim. Acta. 72 (2008) 1611–1625. doi:10.1016/j.gca.2008.01.007.

1085 [96]   A.A. Migdisov, A.E. Williams-Jones, T. Wagner, An experimental study of the solubility
                   and speciation of the Rare Earth Elements (III) in fluoride- and chloride-bearing aqueous
                   solutions at temperatures up to 300°C, Geochim. Cosmochim. Acta. 73 (2009) 7087–
                   7109. doi:10.1016/j.gca.2009.08.023.

1090

Table 1. Concentrations of REE in the initial solution

element	Ce	La	Pr	Nd	Sm	Gd	Y	Tb	Dy	Er	Yb
concentration (ppm)	300	300	35	150	20	20	100	6	45	33	33

Table 2. The thermodynamic properties of LREE(Ca,Ac)PO$_4$ [78,81]

Cation	La	Ce	Pr	Nd	Pm	Sm	Eu	Gd	Ca, Th	Ca,U	
W_x (kJ/mol)		0.8	2.8	5.0	7.6	10.4	13.4	16.5	10.4	10.4	La
			0.6	1.8	3.5	5.6	7.8	10.3	5.6	5.6	Ce
				0.4	1.3	2.6	4.2	6.1	2.6	2.6	Pr
					0.3	1.0	2.1	3.6	1	1	Nd
						0.1	0.8	1.9	0.1	0.1	Pm
							0.2	0.7	0	0	Sm
								0.2	0.2	0.2	Eu
									0.7	0.7	*Gd*
										0	Ca, Th
											Ca,U

Table 3. The thermodynamic properties of HREE(Ca,Ac)PO$_4$.

Cation	**Tb**	**Dy**	**Y**	**Ho**	**Er**	**Tm**	**Yb**	**Lu**	**Ca,Th**	**Ca,U**	
W_x (kJ/mol)		0.16	0.52	0.64	1.41	2.25	3.20	4.62	2.34	0.48	**Tb**
			0.11	0.16	0.63	1.22	1.95	3.08	3.71	1.18	**Dy**
				0.01	0.22	0.61	1.14	2.04	5.07	1.99	**Y**
					0.15	0.49	0.98	1.83	5.43	2.22	**Ho**
						0.10	0.36	0.93	7.39	3.53	**Er**
							0.08	0.42	9.18	4.80	**Tm**
								0.13	11.03	6.16	**Yb**
									13.55	8.07	**Lu**
R_x (Å)	1.040	1.027	1.019	1.015	1.004	0.994	0.985	0.977	1.085[a]	1.060[a]	
V$_x$ (cm³/mol)	43.83[b]	43.35[b]	42.95[c]	42.85[b]	42.37[b]	41.99[b]	41.63[b]	41.19[b]	45.71[d]	44.68[d]	
E_x (GPa)	131.8[e]	146.7[e]	152.0[f]	166.2[g]	173.0[e]	178.0[g]	201.0[h]	202.0[i]			